ACS APPLIED MATERIALS & INTERFACES

Research Article

www.acsami.org

Thiophene-Diketopyrrolopyrrole-Based Quinoidal Small Molecules as Solution-Processable and Air-Stable Organic Semiconductors: Tuning of the Length and Branching Position of the Alkyl Side Chain toward a High-Performance n-Channel Organic Field-Effect Transistor

Chao Wang,[†,‡] Yunke Qin,[†,‡] Yuanhui Sun,[†,‡] Ying-Shi Guan,[†,‡] Wei Xu,*[,†] and Daoben Zhu*[,†]

[†]Beijing National Laboratory for Molecular Sciences, Key Laboratory of Organic Solids, Institute of Chemistry, Chinese Academy of Sciences, Beijing 100190, China

[‡]University of Chinese Academy of Sciences, Beijing 100049, China

Supporting Information

ABSTRACT: A series of thiophene-diketopyrrolopyrrole-based quinoidal small molecules (**TDPPQ-2**–**TDPPQ-5**) bearing branched alkyl chains with different side-chain lengths and varied branching positions are synthesized. Field-effect transistor (FET) measurement combined with thin-film characterization is utilized to systematically probe the influence of the side-chain length and branching position on the film microstructure, molecular packing, and, hence, charge-transport property. All of these **TDPPQ** derivatives show air-stable n-channel transporting behavior in spin-coated FET devices, which exhibit no significant decrease in mobility even after being stored in air for 2 months. Most notably, **TDPPQ-3** exhibits an outstanding n-channel semiconducting property with electron mobilities up to 0.72 $cm^2 V^{-1} s^{-1}$, which is an unprecedented value for spin-coated DPP-based n-type semiconducting small molecules. A balance of high crystallinity, satisfactory thickness uniformity and continuity, and strong intermolecular interaction accounts for the superior charge-transport characteristics of **TDPPQ-3** films. Our study demonstrates that tuning the length and branching position of alkyl side chains of semiconducting molecules is a powerful strategy for achieving high FET performance.

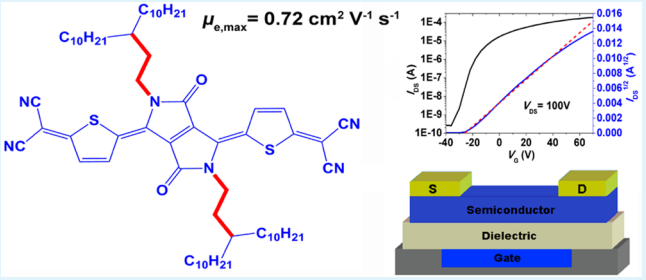

KEYWORDS: *quinoidal molecules, diketopyrrolopyrrole, n-type organic semiconductors, spin-coated OFETs, alkyl-side-chain engineering*

INTRODUCTION

Over the past 2 decades, organic semiconductors (OSCs) have seen considerable development because of their potential application to low-cost, lightweight, and flexible electronic devices, such as organic field-effect transistors (OFETs), organic photovoltaics, and organic light-emitting diodes.[1−7] OFETs, in particular, are expected to open new possibilities for plastic electronic applications including large-area flexible displays, sensors, and radio-frequency identification tags.[8−15]

Generally, solution-processable OSCs are composed of two parts: π-conjugated backbones and branched alkyl side chains. These alkyl chains in semiconducting materials are more than just solubilizing groups. Structural modification of alkyl side chains, such as alterations in length,[16−18] chirality,[19] orientation,[20] density,[21] and branching position,[22−26] can significantly affect intermolecular interaction, molecular packing, and device performance. Recently, more and more research efforts have been devoted to engineering alkyl chains in OSCs.[27,28] Nevertheless, there are very few systematic studies on the influence of the side chain length and branching position on the charge-transport properties of OSCs.[29]

In recent years, n-type OSCs containing diketopyrrolopyrrole (DPP) units have been attracting much interest for their promising features in OFETs.[30−33] The high planarity of DPP and its electron-deficient nature and ability to form hydrogen bonds result in semiconducting materials with strong $\pi-\pi$-stacking interactions and large intramolecular charge transfer.[34−38] Several research groups have reported electron mobility values surpassing 1 $cm^2 V^{-1} s^{-1}$ for FETs based on DPP-containing polymers.[39−42] In comparison, the development of n-type DPP-based small molecules, which possess advantages over polymers including ease of purification and less variation between batches, has largely lagged behind.[43]

Received: May 11, 2015
Accepted: July 2, 2015
Published: July 2, 2015

DOI: 10.1021/acsami.5b04082
ACS Appl. Mater. Interfaces 2015, 7, 15978−15987

Scheme 1. Molecular Structures of TDPPQ-1−TDPPQ-5

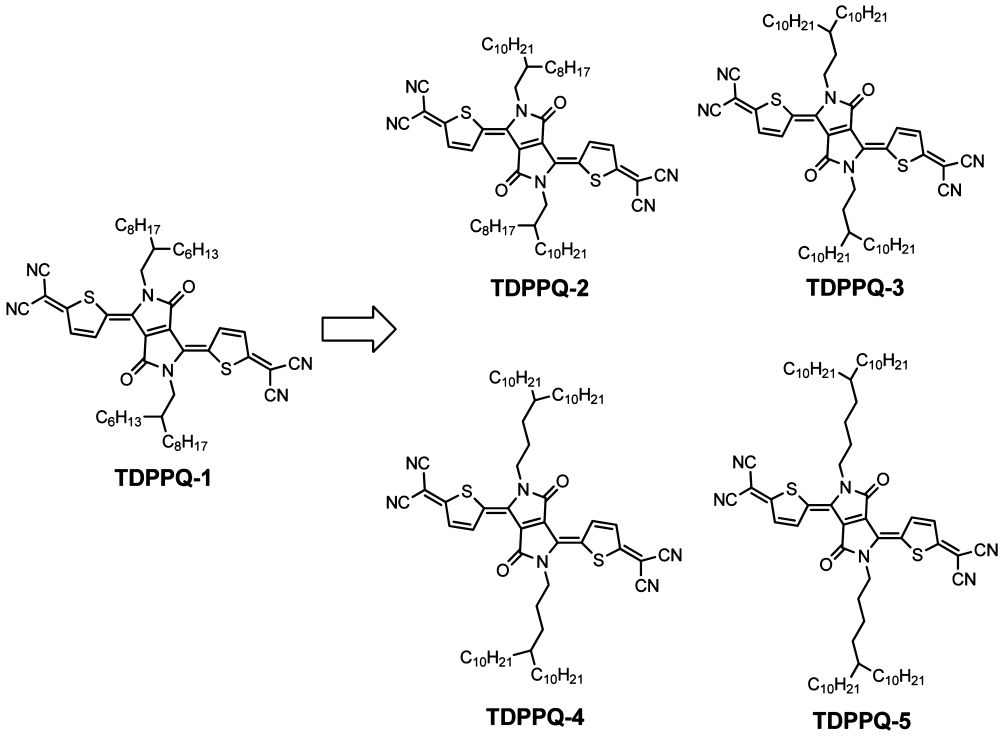

In our search for high-performance n-type OSCs, we focused on DPP-containing quinoidal small molecules with dicyanovinyl terminal groups.[44,45] **TDPPQ-1** is a thiophene-DPP-based n-type OSC reported by our group (Scheme 1).[44] Under ambient conditions, solution-processed FETs based on **TDPPQ-1** exhibited maximum electron mobilities up to 0.35 $cm^2 V^{-1} s^{-1}$. In this report, we designed and synthesized a series of new thiophene-DPP-based quinoidal molecules (**TDPPQs**) with different alkyl side chains (**TDPPQ-2**−**TDPPQ-5**, Scheme 1) and systematically investigated the influence of the side-chain length and branching position on thin-film microstructure, intermolecular interaction, and, hence, device performance. Among these quinoidal molecules, **TDPPQ-3**, with the branching position three carbons away from the DPP core, exhibited the best device performance because a maximum electron mobility of up to 0.72 $cm^2 V^{-1} s^{-1}$ was achieved in spin-coated FETs under an ambient atmosphere. To our knowledge, this is the highest electron mobility for spin-coated n-channel FETs based on DPP-containing small molecules to date.

EXPERIMENTAL SECTION

Materials and General Methods. Chemical reagents were purchased from Sigma-Aldrich, Acros, or Alfa Aesar and used without further purification unless otherwise stated. All of the alkyl iodide compounds were purchased from Lyn (Beijing) Science & Technology Co., Ltd. The synthesis of **TDPPQ-1** was mentioned in our previous report.[44] All air- or moisture-sensitive reactions were carried out under an argon atmosphere. ^1H and ^{13}C NMR spectra were measured on a Bruker Advance 400 MHz spectrometer using $CDCl_3$ as the solvent and tetramethylsilane as the internal standard. All chemical shifts were reported in parts per million, and the data are presented as follows: chemical shift, multiplicity (s = singlet, d = doublet, t = triplet, and m = multiplet), coupling constant in hertz, and integration. Matrix-assisted laser desorption ionization time-of-flight (MALDI-TOF) mass spectrometry (MS) spectra were determined utilizing a Bruker Biflex III MALDI-TOF spectrometer. Elemental analyses were performed with a Carlo Erba 1106 elemental analyzer. Thermogravimetric analysis (TGA) was carried out on a Shimadzu DTG 60 instrument at a heating rate of 10 °C min^{-1} under nitrogen conditions with runs recorded from room temperature to 500 °C. Differential scanning calorimetry (DSC) analysis was performed on a PerkinElmer Pyris 1 instrument under a nitrogen flow at a heating rate of 10 °C min^{-1}, heating from room temperature to 300 °C. Absorption spectra were recorded on a JASCO V-570 UV−vis spectrometer. Cyclic voltammetry (CV) measurements were performed on a CHI660C analyzer with a three-electrode cell under an argon atmosphere, equipped with a platinum disk working electrode, a platinum wire counter electrode, and a Ag/AgCl reference electrode. The supporting electrolyte was an anhydrous dichloromethane solution containing 0.1 mol L^{-1} nBu_4NPF_6. Electron spin resonance (ESR) spectra were obtained with a Bruker EPR ELEXSYS 500 spectrometer. The surface morphology of the films was characterized with a Nanoscope IIIa microscope in tapping mode at ambient temperature. One-dimensional grazing-incidence X-ray diffraction (1D-GIXRD) experiments were recorded on an Empyrean X-ray diffractometer equipped with a Pixcel3D detector by using Cu Kα radiation. Two-dimensional grazing-incidence X-ray diffraction (2D-GIXRD) measurements were carried out at beamline BL14B1, Shanghai Synchrotron Radiation Facility.

Synthesis of TDPPQ-2. Sodium hydride (60% in oil, 0.061 g, 1.52 mmol) was added to a degassed solution of malononitrile (0.050 g, 0.760 mmol) in anhydrous dimethoxyethane (10 mL) at 0 °C under an argon atmosphere, and the resulting suspension was stirred at room temperature for 30 min to give rise to a solution of malononitrile anion. **TDPPBr-2** (0.321 g, 0.315 mmol) and tetrakis-(triphenylphosphine)palladium (0.183 g, 0.158 mmol) were dissolved in dimethoxyethane (10 mL), and then the mixture was heated under reflux for 40 min, followed by the slow addition of the prepared malononitrile anion solution by a syringe. The mixture was refluxed for 7 h and then treated with saturated bromine water (30 mL) at 0 °C. After stirring for 3 h at room temperature, the mixture was extracted with chloroform (50 mL × 3). The combined organic layer was washed with brine and dried over $MgSO_4$. After evaporation of the solvent, the residue was purified by column chromatography on silica gel with toluene/hexane (3:1), followed by recrystallization from

DOI: 10.1021/acsami.5b04082
ACS Appl. Mater. Interfaces 2015, 7, 15978−15987

chloroform/methanol to give **TDPPQ-2** as a dark-green solid (0.159 g, 51%). ^{1}H NMR (400 MHz, $CDCl_3$): δ 9.40 (d, J = 5.7 Hz, 2H), 7.36 (d, J = 5.7 Hz, 2H), 3.98 (d, J = 7.6 Hz, 4H), 1.92 (m, 2H), 1.22−1.35 (m, 64H), 0.83−0.87 (m, 12H). ^{13}C NMR (400 MHz, $CDCl_3$): δ 171.5, 160.4, 146.0, 134.1, 132.5, 130.3, 129.7, 112.2, 111.3, 70.3, 46.1, 37.3, 30.9, 30.8, 29.9, 29.0, 28.6, 28.5, 28.5, 28.3, 28.3, 25.0, 21.7, 21.7, 13.1. MS (MALDI-TOF): m/z 986.5 ([M]$^+$). Anal. Calcd for $C_{60}H_{86}N_6O_2S_2$: C, 72.98; H, 8.78; N, 8.51. Found: C, 72.80; H, 8.76; N, 8.57.

Synthesis of TDPPQ-3. **TDPPQ-3** was prepared according to the same procedure as that for **TDPPQ-2** in 48% yield. ^{1}H NMR (400 MHz, $CDCl_3$): δ 9.37 (d, J = 5.8 Hz, 2H), 7.37 (d, J = 5.7 Hz, 2H), 4.07 (t, J = 7.7 Hz, 4H), 1.61−1.67 (m, 4H), 1.24−1.46 (m, 74H), 0.86 (t, J = 6.4 Hz, 12H). ^{13}C NMR (400 MHz, $CDCl_3$): δ 171.5, 160.0, 145.8, 134.3, 132.2, 130.3, 129.4, 112.1, 111.3, 70.4, 40.6, 34.9, 33.0, 32.4, 30.9, 28.9, 28.6, 28.4, 25.6, 21.7, 13.1. MS (MALDI-TOF): m/z 1070.7 ([M]$^+$). Anal. Calcd for $C_{66}H_{98}N_6O_2S_2$: C, 73.97; H, 9.22; N, 7.84. Found: C, 73.92; H, 9.29; N, 7.88.

Synthesis of TDPPQ-4. **TDPPQ-4** was prepared according to the same procedure as that for **TDPPQ-2** in 45% yield. ^{1}H NMR (400 MHz, $CDCl_3$): δ 9.38 (d, J = 5.8 Hz, 2H), 7.37 (d, J = 5.8 Hz, 2H), 4.02 (t, J = 7.6 Hz, 4H), 1.68 (m, 4H), 1.22−1.37 (m, 78H), 0.86 (t, J = 6.4 Hz, 12H). ^{13}C NMR (400 MHz, $CDCl_3$): δ 171.4, 160.0, 145.8, 134.2, 132.2, 130.4, 129.5, 112.1, 111.2, 70.4, 42.2, 36.0, 32.4, 30.9, 29.4, 29.0, 28.7, 28.7, 28.4, 26.1, 25.6, 21.7, 13.1. MS (MALDI-TOF): m/z 1098.8 ([M]$^+$). Anal. Calcd for $C_{68}H_{102}N_6O_2S_2$: C, 74.27; H, 9.35; N, 7.64. Found: C, 74.32; H, 9.45; N, 7.73.

Synthesis of TDPPQ-5. **TDPPQ-5** was prepared according to the same procedure as that for **TDPPQ-2** in 44% yield. ^{1}H NMR (400 MHz, $CDCl_3$): δ 9.38 (d, J = 5.8 Hz, 2H), 7.37 (d, J = 5.8 Hz, 2H), 4.06 (t, J = 7.6 Hz, 4H), 1.66−1.71 (m, 4H), 1.20−1.39 (m, 82H), 0.86 (t, J = 6.3 Hz, 12H). ^{13}C NMR (400 MHz, $CDCl_3$): δ 171.5, 160.0, 145.8, 134.2, 132.2, 130.4, 129.5, 112.1, 111.3, 70.4, 41.8, 36.2, 32.5, 32.2, 30.9, 29.3, 29.1, 28.7, 28.7, 28.4, 25.7, 22.9, 21.7, 13.1. MS (MALDI-TOF): m/z 1126.8 ([M]$^+$). Anal. Calcd for $C_{70}H_{106}N_6O_2S_2$: C, 74.55; H, 9.47; N, 7.45. Found: C, 74.57; H, 9.51; N, 7.51.

FET Device Fabrication and Measurement. OFETs were fabricated in the bottom-gate/top-contact (BGTC) configuration. A heavily n-doped silicon (Si) wafer and a 300 nm thermally oxidized SiO_2 layer (capacitance per unit area C_i = 11 nF/cm^2) were utilized as the gate electrode and dielectric layer, respectively. The cleaned SiO_2/Si substrate was modified with octadecyltrichlorosilane (OTS) to form a self-assembled monolayer. The semiconducting layer was deposited on the OTS-treated substrate by spin coating of a 10 mg mL^{-1} chloroform solution with a speed of 6000 rpm under an ambient atmosphere, followed by thermal annealing under vacuum conditions at different temperatures for 30 min. Gold source−drain electrodes with a thickness of 30 nm were deposited on a semiconducting layer by vacuum evaporation through a shadow mask. The drain−source channel length (L) and width (W) were 25 and 200 μm, respectively. All FET devices were tested under ambient conditions using a Keithley 4200 parameter analyzer on a probe stage. The carrier mobility, μ, was determined in the saturation regime from the equation $I_{DS} = (W/2L)C_i\mu(V_G - V_T)^2$, where I_{DS} denotes the drain−source current in the saturated regime, W and L are the channel width and length, respectively, C_i is the capacitance per unit area of the gate dielectric layer, and V_G and V_T are the gate voltage and threshold voltage, respectively.

RESULTS AND DISCUSSION

Synthesis and Photophysical Properties. The syntheses of **TDPPQ-2**−**TDPPQ-5** are outlined in Scheme 2. These compounds possess the same conjugated backbone as **TDPPQ-1** does, but their branched alkyl side chains vary in their length and branching position. In comparison to **TDPPQ-1**, **TDPPQ-2** has longer alkyl side chains, with the same branching point at the second carbon position. By contrast, the side chains of **TDPPQ-3**, **TDPPQ-4**, and **TDPPQ-5** are not only increased

Scheme 2. Synthesis of Target Compounds TDPPQ-2−TDPPQ-5

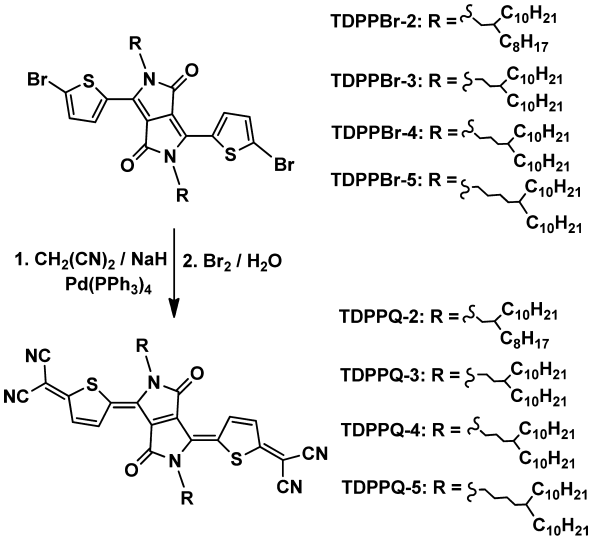

in length but branched at the third, fourth, and fifth carbons away from the conjugated backbone, respectively. The preparation of dibromo-substituted precursors **TDPPBr-2**−**TDPPBr-5** is shown in detail in the Supporting Information (SI). Starting from the corresponding precursors, the **TDPPQs** were synthesized through a palladium-catalyzed Takahashi coupling reaction,[46,47] followed by oxidation with saturated bromine water in moderate yields. Their chemical structures were fully characterized by NMR, MALDI-TOF MS, and elementary analysis. Because of the long and branched alkyl chains, all of the compounds exhibit high solubilities (>10 mg mL^{-1}) in common organic solvents such as chloroform, dichloromethane, chlorobenzene, dichlorobenzene, and toluene. TGA shows that the thermolysis onset temperatures for **TDPPQ-2**−**TDPPQ-5** are 317, 325, 326, and 328 °C, respectively (Figure S1 in the SI). In addition, DSC analysis shows that obvious melting points for **TDPPQ-2**−**TDPPQ-5** were observed at 193, 184, 195, and 187 °C respectively (Figure S2 in the SI), indicating the presence of an odd−even effect in melting points for these quinoidal molecules with different branching positions. The TGA and DSC data suggest that **TDPPQs** possess good thermal stability, enabling analysis of thin-film crystallinity and morphology over a broad range of annealing temperatures.

UV−vis absorption spectra of **TDPPQs** are shown in Figure 1. In dilute dichloromethane solutions, the absorptions of **TDPPQs** (Figure 1a) were nearly identical with the maximum absorption band (0−0 vibrational peak) at 642 nm, suggesting that the alkyl chains have a negligible influence on the photophysical properties of the conjugated backbone. All of the compounds possess similar optical band gaps (E_g) of 1.72−1.73 eV (Table S1 in the SI), estimated from the absorption edges. The temperature has very little effect on the absorption spectra of **TDPPQs** in solution. As depicted in Figure S3 in the SI, the compounds **TDPPQ-4** and **TDPPQ-5** displayed identical absorption spectra in toluene at various temperatures from 0 to 75 °C. In the thin films, the absorption spectra of **TDPPQ-1**−**TDPPQ-5** (Figure 1b) are broadened relative to the corresponding solution spectra, and the 0−0 vibrational peaks are red-shifted by 82, 82, 114, 102, and 98 nm, respectively, because of intermolecular π−π stacking in the solid state. The

DOI: 10.1021/acsami.5b04082
ACS Appl. Mater. Interfaces 2015, 7, 15978−15987

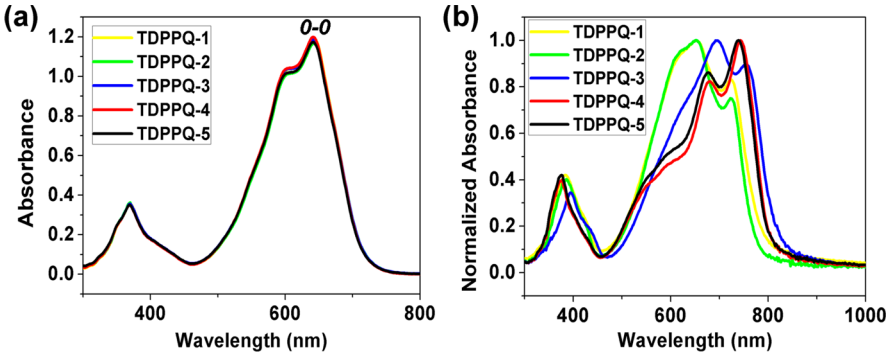

Figure 1. UV−vis absorption spectra of **TDPPQ-1**−**TDPPQ-5**. (a) Dichloromethane solutions at room temperature. (b) Thin films on quartz substrates at room temperature.

thin-film absorption peaks of **TDPPQ-1** and **TDPPQ-2** appear at almost the same wavelength and their shapes are similar, suggesting that the effect of the side-chain length on molecular packing is not very significant. **TDPPQ-3**, which differs from any other compound in spectral shape, exhibits the most red-shifted absorption bands of **TDPPQ**s in the solid state. This observation indicates that subtle changes in the side-chain branching position can greatly affect molecular packing, and an alkyl chain branched at the third carbon position results in the strongest intermolecular $\pi-\pi$ interaction. The change in the alkyl chain branching position in **TDPPQ-4** compared to **TDPPQ-3** also has a dramatic influence on the shape and wavelength of the absorption profile. However, further movement of the branching point away from the backbone did not cause a significant change in thin-film absorption wavelength and spectral shape from **TDPPQ-4** to **TDPPQ-5**. The films of **TDPPQ-1**−**TDPPQ-5** were treated by thermal annealing to improve the order of molecules in these films. As shown in Figure S4 in the SI, the absorption spectra of all **TDPPQ** derivatives undergo very small changes with increasing annealing temperature from room temperature to 150 °C, indicating that the molecular packing patterns in the as-spun films of these compounds were highly ordered. However, the spectrum of the **TDPPQ-3** film features a significant red shift and broadening after annealing at 180 °C.

Redox Behavior. CV (Figure 2) measurements were conducted to investigate the redox behavior of compounds **TDPPQ2**−**TDPPQ-5**. All of the compounds exhibited similar redox behavior with two well-resolved reversible reduction peaks, but no oxidation peak was observed. The lowest unoccupied moleuclar orbital (LUMO) and highest occupied moleuclar orbital (HOMO) energies calculated from the data of CV and absorption spectra are −4.50 to −4.52 eV and −6.22 to −6.25 eV (Table S1 in the SI), indicating that the side-chain engineering has no significant influence on the redox properties of **TDPPQ**s.

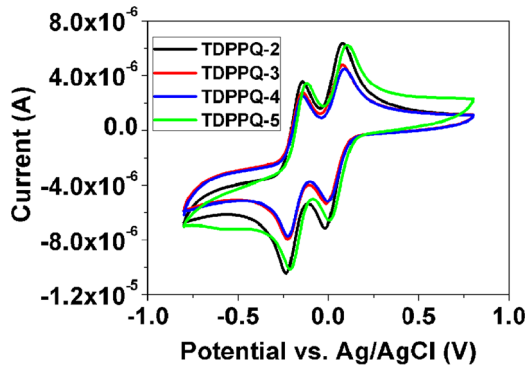

Figure 2. Cyclic voltammograms of **TDPPQ-2**−**TDPPQ-5** with 0.1 mol L^{-1} *n*-Bu_4NPF_6 in dichloromethane solutions under a scan rate of 50 mV s^{-1}.

CV analysis showed that **TDPPQ**s displayed reversible two-stage reduction behaviors, and this redox property was further confirmed by a stepwise reduction of **TDPPQ-3** with tetrabutylammonium ($TBABH_4$). In the course of stepwise reductive titration, sequential reduction to the radical anion and then the dianion was observed. When a dichloromethane solution of **TDPPQ-3** was titrated with $TBABH_4$, the absorption peaks of the radical anion appeared in the UV−vis spectrum at 980, 872, 780, 430, and 364 nm (Figure S5a in the SI). The formation of the radical anion was confirmed by an ESR spectrum exhibiting a sharp signal (Figure S6 in the SI). Further titration led to the appearance of dianion absorption peaks at 710 and 344 nm (Figure S5b in the SI). After the addition of 2 equiv or more of a reducing reagent, the UV−vis spectrum showed exclusive formation of a dianion, which was ESR-silent.

OFET Characterization. To investigate how our side-chain engineering affects the charge-transport properties of **TDPPQ**s, we fabricated BGTC OFET devices. The thin films of **TDPPQ-2**−**TDPPQ-5** were deposited on top of the octadecyltrimethoxysilane (OTS)-treated SiO_2/Si substrates by spin coating of a chloroform solution. All of the thin-film devices were fabricated and measured under ambient conditions, and the mobility values were calculated from the transfer characteristics in the saturation regime. For comparison, the device of **TDPPQ-1** was also fabricated and characterized under exactly the same conditions as those of new **TDPPQ** derivatives. Typical transfer and output curves are displayed in Figures 3 and S7 in the SI, and the OFET results are collected in Table 1. It can be seen that **TDPPQ**s exhibited electron-transport characteristics regardless of the length or branching position of the side chain. FET devices based on **TDPPQ-1** displayed a maximum electron mobility of 0.33 cm^2 V^{-1} s^{-1}. By contrast, the thin films of **TDPPQ-2** exhibited decreased mobility: a maximum mobility of 0.25 cm^2 V^{-1} s^{-1} was observed upon thermal annealing at 120 °C. For **TDPPQ-3**, an exciting device performance with maximum electron mobility up to 0.72 cm^2 V^{-1} s^{-1}, more than twice that of **TDPPQ-1**, was achieved after annealing at 150 °C. To the best of our knowledge, this electron mobility value is a new record for spin-coated DPP-containing n-type small molecules. As for **TDPPQ-4** and

DOI: 10.1021/acsami.5b04082
ACS Appl. Mater. Interfaces 2015, 7, 15978−15987

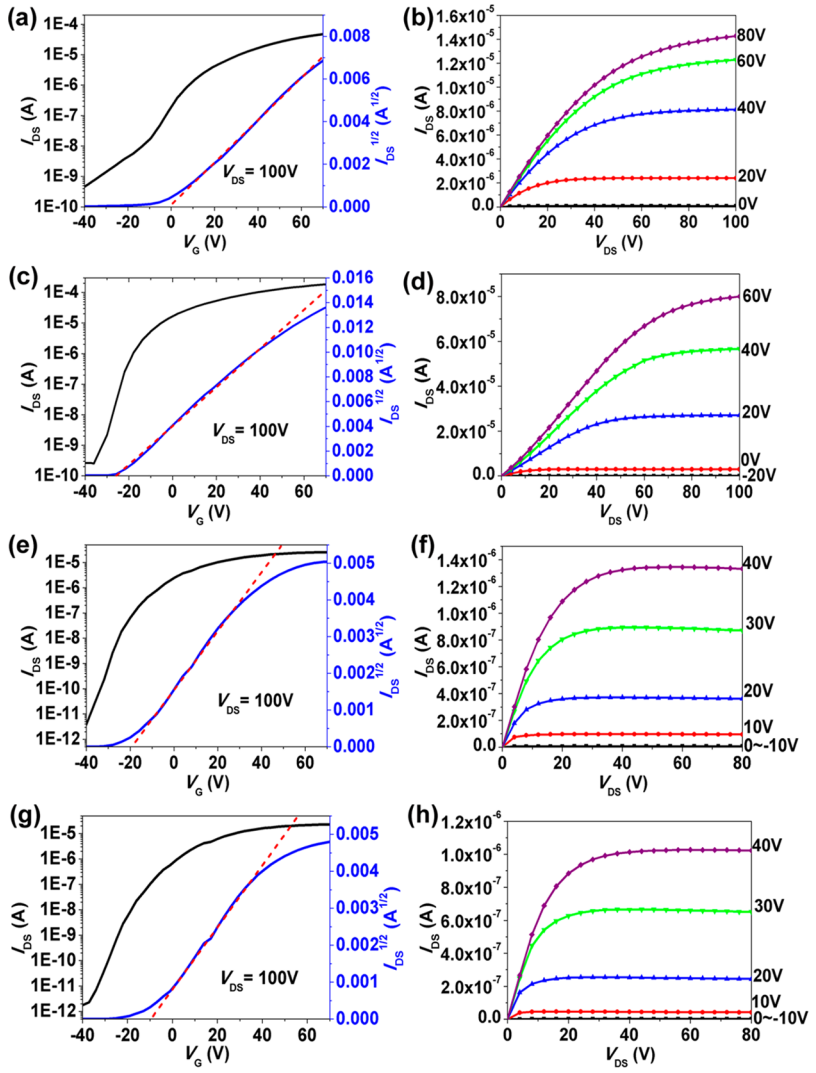

Figure 3. Transfer and output characteristics of BGTC OFETs based on **TDPPQ-2** (a and b), **TDPPQ-3** (c and d), **TDPPQ-4** (e and f), and **TDPPQ-5** (g and h). Devices based on **TDPPQ-2** and **TDPPQ-3** were annealed at 120 and 150 °C, respectively, and devices based on **TDPPQ-4** and **TDPPQ-5** were fabricated with as-deposited films. Red dashed lines in parts a, c, e, and g indicate fits used to extract the mobility values.

TDPPQ-5, the as-deposited thin-film transistors showed optimum performance with maximum electron mobilities of 0.21 and 0.19 $cm^2\ V^{-1}\ s^{-1}$, respectively, which are much lower compared to that of a **TDPPQ-3**-based device. All of these devices exhibited no significant decrease in mobility after being stored under ambient conditions for 2 months (Figure S8 in the SI), suggesting the excellent air stability of the **TDPPQ** transistors. Although the charge traps can be reduced by OTS, they cannot be completely eliminated. Obvious hysteresis was observed in the transfer curves of FET devices based on **TDPPQ**s (Figure S9 in the SI). In OFETs, the device performance not only is dependent on the intrinsic electrical properties of semiconducting molecules but also is affected by the work function of the electrodes. Silver, whose work function is lower than that of gold, is also a common metal for electrode applications. Thus, silver was also employed as source and drain electrodes in OFET devices based on the optimized films of **TDPPQ-3**. As a result, a maximum electron mobility of about 0.10 $cm^2\ V^{-1}\ s^{-1}$ (Figure S10 in the SI), much lower than that of the devices with gold electrodes, was achieved in the FETs with silver electrodes.

The dependence of the device performance of **TDPPQ**s on the annealing temperature was further studied. As shown in Table 1, the devices of **TDPPQ-1** and **TDPPQ-2** showed a stepwise increase in mobility with increasing annealing temperature from 90 to 120 °C. As for **TDPPQ-3**, the as-deposited thin film showed a high mobility of 0.36 $cm^2\ V^{-1}\ s^{-1}$, and the mobility increased stepwise to a maximum value of 0.72 $cm^2\ V^{-1}\ s^{-1}$ with increasing annealing temperature up to 150 °C, indicating that **TDPPQ-3** is a promising candidate for n-type OSCs. Compared with other **TDPPQ** derivatives, both **TDPPQ-4** and **TDPPQ-5** showed a much different phenomenon, with the as-deposited devices displaying high mobilities (~0.2 $cm^2\ V^{-1}\ s^{-1}$), which decreased steadily with increasing annealing temperature.

Thin-Film Microstructure. To gain further understanding of the charge-transport behavior of **TDPPQ**s, we utilized atomic force microscopy (AFM) and out-of-plane 1D-GIXRD to investigate film morphologies and molecular packings. Figure 4 shows the AFM images of thin films of **TDPPQ**s annealed at different temperatures. The as-deposited films of **TDPPQ-2**, **TDPPQ-4**, and **TDPPQ-5** appeared continuous and relatively uniform with small domains, while the as-deposited film of

DOI: 10.1021/acsami.5b04082
ACS Appl. Mater. Interfaces 2015, 7, 15978−15987

Table 1. Device Performance of OFETs Based on TDPPQs

compd	T (°C)[a]	mobility ($cm^2\ V^{-1}\ s^{-1}$)[b]	I_{on}/I_{off}[b]	threshold voltage (V)[b]
TDPPQ-1	RT	0.15 ± 0.04	10^4	2.3−7.3
	90	0.20 ± 0.01	10^4	6.8−9.0
	120	0.28 ± 0.05	10^6−10^7	4.1−7.4
	150	0.12 ± 0.03	10^3−10^4	5.0−7.5
TDPPQ-2	RT	0.075 ± 0.015	10^5	0.1−1.2
	90	0.12 ± 0.03	10^5	2.0−5.6
	120	0.21 ± 0.04	10^5	0.7−3.8
	150	0.03 ± 0.03	10^4−10^5	−4.0 to −0.8
TDPPQ-3	RT	0.32 ± 0.04	10^4−10^5	−11.5 to −5.1
	90	0.45 ± 0.02	10^4−10^5	−21.5 to −18.5
	120	0.56 ± 0.05	10^4	−25.0 to −14.3
	150	0.69 ± 0.03	10^5	−23.0 to −16.5
	180	0.16 ± 0.03	10^3	−35.5 to −27.7
TDPPQ-4	RT	0.19 ± 0.02	10^6	−18.9 to −8.4
	90	0.14 ± 0.03	10^5	−23.8 to −15.1
	120	0.10 ± 0.01	10^4−10^5	−24.5 to −22.8
	150	0.081 ± 0.018	10^4	−27.6 to −23.2
TDPPQ-5	RT	0.16 ± 0.03	10^6	−11.1 to −6.8
	90	0.11 ± 0.04	10^6	−23.5 to −14.2
	120	0.095 ± 0.005	10^5	−20.0 to −18.5
	150	0.078 ± 0.019	10^5	−20.8 to −14.3

[a]Annealing temperature. [b]The device characteristics were obtained from more than 10 devices for each material, and all devices were measured under ambient conditions.

TDPPQ-3 exhibited a fibrillar network of granular features, suggesting good crystallinity of **TDPPQ-3**. All of the thin-film morphologies of **TDPPQ** derivatives underwent obvious changes after annealing treatment, and the domains grew in size with increasing annealing temperature. For **TDPPQ-2**, the films annealed at 90 and 120 °C remained continuous and uniform, but a rough morphology was observed for the film after annealing at 150 °C. **TDPPQ-3** films annealed at 90−150 °C displayed steadily enhanced uniformity and continuity with increasing grain size, and an ordered film with large domain size and relatively uniform surface was successfully obtained when annealed at 150 °C. However, when the annealing temperature further increased to 180 °C, the grain boundaries of the **TDPPQ-3** film were increased dramatically, which showed a negative influence on the charge-transport property. For the films of **TDPPQ-4** and **TDPPQ-5**, the intergrain boundaries and surface roughnesses were continuously increased as the annealing temperature increased, consistent with a stepwise decrease in the electron mobility.

Figures 5 and S11 in the SI show 1D-GIXRD patterns of the spin-coated thin films of **TDPPQ** derivatives annealed at different temperatures. On the whole, the intensity of diffraction peaks was steadily enhanced with increased annealing temperature, indicating increasing crystallinity. In comparison with the film of **TDPPQ-1**,[44] **TDPPQ-2**-based films showed less crystallinity, with only one weak diffraction peak (2θ = 3.2°) observable, owing to the prolonged side chain of **TDPPQ-2**. The d spacing estimated from this peak was 27.6 Å, which is larger than that of **TDPPQ-1** (24.0 Å). **TDPPQ-3** films exhibited sharp diffraction peaks up to third order, and the d spacing estimated from the strong (001) peak was 33.5 Å. Interestingly, an additional new peak at 2θ of 3.1° was observed, suggesting that a new phase appeared in the thin films. These diffraction peaks indicate that **TDPPQ-3** with the branching position three carbons away from the conjugation backbone exhibits a high degree of crystallinity in the films, which is consistent with the high device performance. Compared with **TDPPQ-3**, **TDPPQ-4** and **TDPPQ-5** appeared much less crystalline, presumably attributed to their longer side chains. For **TDPPQ-4** films, GIXRD patterns displayed a strong (001) peak (2θ = 4.1°) and a weak (002) peak (2θ = 8.2°). **TDPPQ-5** films showed only one diffraction peak (2θ = 4.0°) at different annealing temperatures. The poorer crystallinity for **TDPPQ-4** and **TDPPQ-5** may account

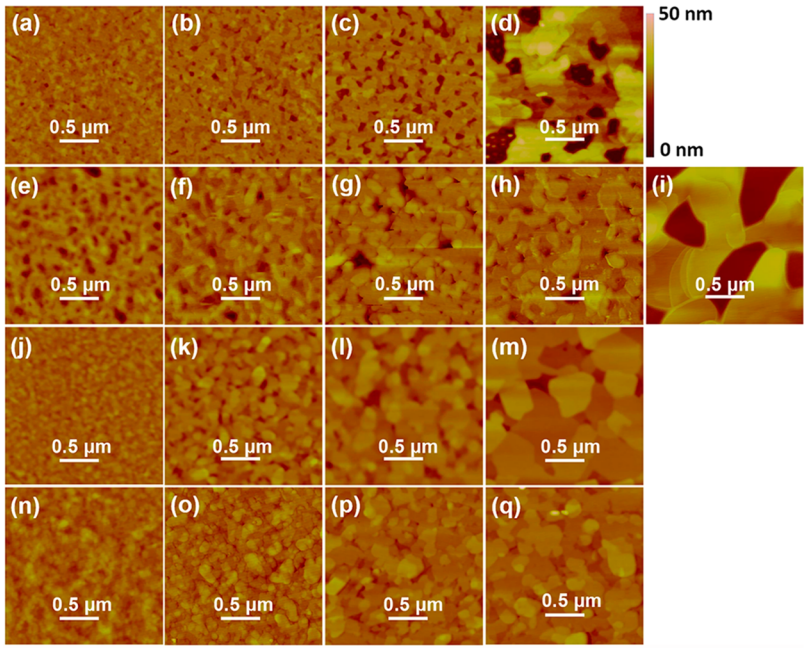

Figure 4. AFM images (2 μm × 2 μm) of thin films of (a−d) **TDPPQ-2**, (e−i) **TDPPQ-3**, (j−m) **TDPPQ-4**, and (n−q) **TDPPQ-5** after annealing at temperatures of (a, e, j, and n) RT, (b, f, k, and o) 90 °C, (c, g, l, and p) 120 °C, (d, h, m, and q) 150 °C, and (i) 180 °C.

DOI: 10.1021/acsami.5b04082
ACS Appl. Mater. Interfaces 2015, 7, 15978−15987

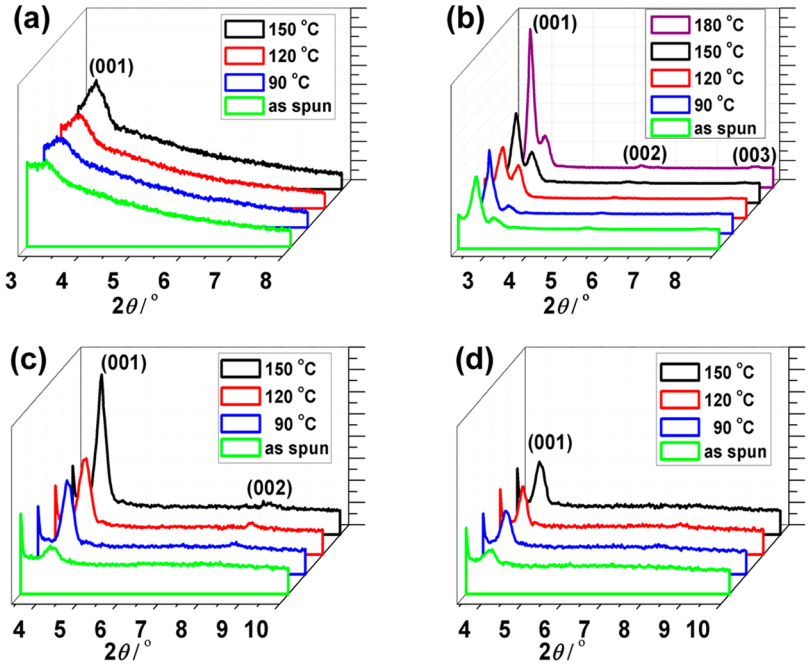

Figure 5. 1D-GIXRD patterns of thin films of (a) **TDPPQ-2**, (b) **TDPPQ-3**, (c) **TDPPQ-4**, and (d) **TDPPQ-5** after annealing at different temperatures.

for their lower device performance compared to **TDPPQ-3**. In addition, their higher volume fraction of insulating side chains relative to **TDPPQ-3** may also contribute to their lower device performance. Many reports have revealed that longer alkyl side chains are detrimental to field-effect mobility because of the larger insulating volume.[48,49] The *d*-spacing values of **TDPPQ-4** and **TDPPQ-5** are 21.4 and 22.1 Å, respectively, even smaller than that of **TDPPQ-1**. Unlike **TDPPQ-2** and **TDPPQ-3**, the *d* spacings of **TDPPQ-4** and **TDPPQ-5** do not correlate well with their alkyl chain lengths, indicating that side chains of these two compounds adopt a different extended conformation in films compared to other **TDPPQ** derivatives. 1D-GIXRD patterns of **TDPPQ**s demonstrate that both the branched alkyl chain length and branching position have an influence on the thin-film crystallinity, and a branched alkyl chain with the appropriate branching position and length may lead to excellent film crystallinity and, hence, high FET performance.

Because single crystals of **TDPPQ** derivatives are difficult to grow because of their long branched alkyl side chains, two-dimensional grazing-incidence X-ray diffraction (2D-GIXRD) measurements were employed to further investigate intermolecular stacking. 2D-GIXRD measurements were carried out on the thin films of **TDPPQ**s corresponding to optimum device performance (Figure 6). The 2D-GIXRD patterns are characterized by a series of out-of-plane peaks along q_z, which are well consistent with the diffraction peaks observed in 1D-GIXRD patterns. By tuning the position of the 2D detector, we observed a diffraction peak in the in-plane direction (q_{xy}) with a distance of about 3.4 Å for the **TDPPQ-3** film (Figure S12 in the SI), which likely corresponds to $\pi-\pi$ stacking of **TDPPQ-3**. Such a small $\pi-\pi$ distance suggests that the strong intermolecular interactions exist in the film of **TDPPQ-3**, well correlated with the thin-film absorption spectra of **TDPPQ-3**. Unfortunately, we did not observe any diffraction peaks along q_{xy} for the films of other **TDPPQ** derivatives by tuning the detector position.

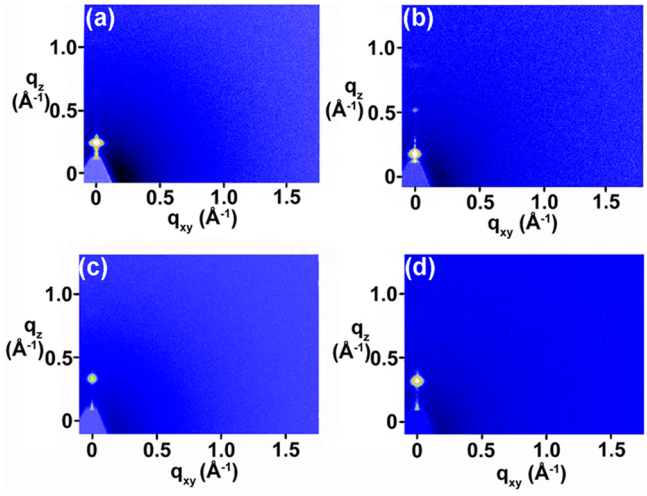

Figure 6. 2D-GIXRD patterns for optimized thin films of (a) **TDPPQ-2**, (b) **TDPPQ-3**, (c) **TDPPQ-4**, and (d) **TDPPQ-5**.

Theoretical calculation at the B3LYP/6-31G* level was performed to probe the packing mode of thin films of **TDPPQ**s. Theoretically optimized structures of **TDPPQ**s are displayed in Figure S13 in the SI. According to the theoretical results, the estimated molecular lengths of **TDPPQ-1**–**TDPPQ-5** are 25, 28, 33, 35, and 38 Å, respectively. Comparing the lengths of **TDPPQ**s with the corresponding *d* spacings derived from 1D-GIXRD patterns, we found that the molecular lengths of **TDPPQ-1**–**TDPPQ-3** are well in agreement with the corresponding monolayer thicknesses in the films. Considering the similarity and compatibility of the alkyl groups with OTS-modified SiO_2/Si substrates, we believe that **TDPPQ-1**–**TDPPQ-3** tend to present an end-to-end packing mode on the substrate along the alkyl stretching directions in thin films. However, the *d* spacings of **TDPPQ-4** and **TDPPQ-5** films are much shorter than the corresponding

DOI: 10.1021/acsami.5b04082
ACS Appl. Mater. Interfaces 2015, 7, 15978–15987

molecular lengths, suggesting that the side chains are closely interdigitated with the other side chains in adjacent layers, which correspond to the interdigitation packing mode. A special change in the thin-film morphology and, hence, in the electron mobility with increasing annealing temperature for **TDPPQ-4** and **TDPPQ-5** could be ascribed to their packing mode, which is different from that of other **TDPPQ** derivatives.

CONCLUSION

We have developed a series of thiophene-DPP-based quinoidal molecules (**TDPPQ-2**−**TDPPQ-5**) having branched alkyl side chains with different lengths and branching positions. OFET measurement was combined with thin-film characterization (UV−vis, AFM, 1D-GIXRD, and 2D-GIXRD) to investigate the influence of the side-chain length and branching position on the film microstructure, molecular packing, and, hence, device performance. All of these quinoidal molecules exhibited air-stable n-channel semiconducting characteristics, and their FET devices showed no significant decrease in mobility after storage under an ambient atmosphere for 2 months. **TDPPQ-1** and **TDPPQ-2** shared a similar molecular packing but showed obvious differences in their film crystallinity and electron mobility, suggesting a moderate effect of the side-chain length on the lamellar ordering of the film and, hence, device performance. With an alkyl chain branched at the third carbon position, **TDPPQ-3** exhibited high film crystallinity, satisfactory film uniformity and continuity, and close in-plane stacking, indicating that subtle changes in the side-chain branching position can greatly improve the film quality and molecular packing. The devices based on **TDPPQ-3** displayed an exciting device performance, with electron mobilities up to 0.72 $cm^2 V^{-1} s^{-1}$, which is a record value for spin-coated n-channel FETs based on DPP-containing small molecules. However, movement of the branching side-chain position away from the backbone does not always improve the film quality and device performance. **TDPPQ-4** and **TDPPQ-5** showed much poorer crystallinity and significantly lower electron mobility compared to **TDPPQ-3**, which may be attributed to their longer side chains. These results suggest that possessing a branched alkyl side chain with the appropriate length and branching position for semiconducting molecules plays a vital role in achieving a balance of high film crystallinity, satisfactory layer uniformity and continuity, and efficient molecular stacking, which results in excellent charge-transport property.

ASSOCIATED CONTENT

Supporting Information

Detailed synthetic procedures for the preparation of **TDPPBr-2**−**TDPPBr-5**, TGA, DSC, optical absorption, and electrochemical data, absorption spectra of **TDPPQ-4** and **TDPPQ-5** in toluene at different temperatures, UV−vis spectra of thin films after thermal annealing, absorption spectral change in the reductive titration of **TDPPQ-3**, ESR spectrum of the radical anion of **TDPPQ-3**, OFET performance of **TDPPQ-1**, air-stability measurements, hysteresis effect of **TDPPQ** devices, the optimum performance of **TDPPQ-3** devices with Ag electrodes, 2D-GIXRD patterns of **TDPPQ-3**-based films, theoretically optimized structures of **TDPPQ**, and NMR spectra. The Supporting Information is available free of charge on the ACS Publications website at DOI: 10.1021/acsami.5b04082.

AUTHOR INFORMATION

Corresponding Authors

*E-mail: wxu@iccas.ac.an.
*E-mail: zhudb@iccas.ac.cn.

Notes

The authors declare no competing financial interest.

ACKNOWLEDGMENTS

This work was supported by the National Natural Science Foundation of China (Grants 21290191 and 21333011), National Basic Research Program of China (Grant 2011CB808401), and the Strategic Priority Research Program of the Chinese Academy of Sciences (Grant XDB12000000). The 2D-GIXRD data were obtained at the Shanghai Synchrotron Facility. The authors thank the assistance of scientists of beamline BL14B1 during the experiments.

REFERENCES

(1) Takimiya, K.; Shinamura, S.; Osaka, I.; Miyazaki, E. Thienoacene-Based Organic Semiconductors. *Adv. Mater.* **2011**, *23*, 4347−4370.
(2) Jiang, W.; Li, Y.; Wang, Z. Heteroarenes as High Performance Organic Semiconductors. *Chem. Soc. Rev.* **2013**, *42*, 6113−6127.
(3) Lee, J.; Jang, M.; Lee, S. M.; Yoo, D.; Shin, T. J.; Oh, J. H.; Yang, C. Fluorinated Benzothiadiazole (BT) Groups as a Powerful Unit for High-Performance Electron-Transporting Polymers. *ACS Appl. Mater. Interfaces* **2014**, *6*, 20390−20399.
(4) Mas-Torrent, M.; Rovira, C. Novel Small Molecules for Organic Field-Effect Transistors: towards Processability and High Performance. *Chem. Soc. Rev.* **2008**, *37*, 827−838.
(5) Segura, J. L.; Martín, N.; Guldi, D. M. Materials for Organic Solar Cells: the C_{60}/π-Conjugated Oligomer Approach. *Chem. Soc. Rev.* **2005**, *34*, 31−47.
(6) Wang, Q.; Ma, D. Management of Charges and Excitons for High-Performance White Organic Light-Emitting Diodes. *Chem. Soc. Rev.* **2010**, *39*, 2387−2398.
(7) Usta, H.; Facchetti, A.; Marks, T. J. N-Channel Semiconductor Materials Design for Organic Complementary Circuits. *Acc. Chem. Res.* **2011**, *44*, 501−510.
(8) Gelinck, G. H.; Huitema, H. E. A.; van Veenendaal, E.; Cantatore, E.; Schrijnemakers, L.; van der Putten, J. B. P. H.; Geuns, T. C. T.; Beenhakkers, M.; Giesbers, J. B.; Huisman, B.-H.; Meijer, E. J.; Benito, E. M.; Touwslager, F. J.; Marsman, A. W.; van Rens, B. J. E.; de Leeuw, D. M. Flexible Active-Matrix Displays and Shift Registers Based on Solution-Processed Organic Transistors. *Nat. Mater.* **2004**, *3*, 106−110.
(9) Arias, A. C.; MacKenzie, J. D.; McCulloch, I.; Rivnay, J.; Salleo, A. Materials and Applications for Large Area Electronics: Solution-Based Approaches. *Chem. Rev.* **2010**, *110*, 3−24.
(10) Berggren, M.; Nilsson, D.; Robinson, N. D. Organic Materials for Printed Electronics. *Nat. Mater.* **2007**, *6*, 3−5.
(11) Roberts, M. E.; Sokolov, A. N.; Bao, Z. Material and Device Considerations for Organic Thin-Film Transistor Sensors. *J. Mater. Chem.* **2009**, *19*, 3351−3363.
(12) Gelinck, G.; Heremans, P.; Nomoto, K.; Anthopoulos, T. D. Organic Transistors in Optical Displays and Microelectronic Applications. *Adv. Mater.* **2010**, *22*, 3778−3798.
(13) Andersson, P.; Forchheimer, R.; Tehrani, P.; Berggren, M. Printable All-Organic Electrochromic Active-Matrix Displays. *Adv. Funct. Mater.* **2007**, *17*, 3074−3082.
(14) Baude, P. F.; Ender, D. A.; Haase, M. A.; Kelley, T. W.; Muyres, D. V.; Theiss, S. D. Pentacene-Based Radio-Frequency Identification Circuitry. *Appl. Phys. Lett.* **2003**, *82*, 3964−3966.
(15) Janata, J.; Josowicz, M. Conducting Polymers in Electronic Chemical Sensors. *Nat. Mater.* **2003**, *2*, 19−24.
(16) McCulloch, I.; Heeney, M.; Bailey, C.; Genevicius, K.; MacDonald, I.; Shkunov, M.; Sparrowe, D.; Tierney, S.; Wagner, R.; Zhang, W.; Chabinyc, M. L.; Kline, R. J.; McGehee, M. D.; Toney, M.

DOI: 10.1021/acsami.5b04082
ACS Appl. Mater. Interfaces 2015, 7, 15978−15987

F. Liquid-Crystalline Semiconducting Polymers with High Charge-Carrier Mobility. *Nat. Mater.* **2006**, *5*, 328−333.
(17) Osaka, I.; Zhang, R.; Sauvé, G.; Smilgies, D.-M.; Kowalewski, T.; McCullough, R. D. High-Lamellar Ordering and Amorphous-Like π-Network in Short-Chain Thiazolothiazole-Thiophene Copolymers Lead to High Mobilities. *J. Am. Chem. Soc.* **2009**, *131*, 2521−2529.
(18) Chen, H.; Guo, Y.; Yu, G.; Zhao, Y.; Zhang, J.; Gao, D.; Liu, H.; Liu, Y. Highly π-Extended Copolymers with Diketopyrrolopyrrole Moieties for High-Performance Field-Effect Transistors. *Adv. Mater.* **2012**, *24*, 4618−4622.
(19) Torsi, L.; Farinola, G. M.; Marinelli, F.; Tanese, M. C.; Omar, O. H.; Valli, L.; Babudri, F.; Palmisano, F.; Zambonin, P. G.; Naso, F. A Sensitivity-Enhanced Field-Effect Chiral Sensor. *Nat. Mater.* **2008**, *7*, 412−417.
(20) Wu, Q.; Ren, S.; Wang, M.; Qiao, X.; Li, H.; Gao, X.; Yang, X.; Zhu, D. Alkyl Chain Orientations in Dicyanomethylene-Substituted 2,5-Di(thiophen-2-yl)thieno-[3,2-b]thienoquinoid: Impact on Solid-State and Thin-Film Transistor Performance. *Adv. Funct. Mater.* **2013**, *23*, 2277−2284.
(21) Kline, R. J.; DeLongchamp, D. M.; Fischer, D. A.; Lin, E. K.; Richter, L. J.; Chabinyc, M. L.; Toney, M. F.; Heeney, M.; McCulloch, I. Critical Role of Side-Chain Attachment Density on the Order and Device Performance of Polythiophenes. *Macromolecules* **2007**, *40*, 7960−7965.
(22) Lei, T.; Dou, J.-H.; Pei, J. Influence of Alkyl Chain Branching Positions on the Hole Mobilities of Polymer Thin-Film Transistors. *Adv. Mater.* **2012**, *24*, 6457−6461.
(23) Dou, J.-H.; Zheng, Y.-Q.; Lei, T.; Zhang, S.-D.; Wang, Z.; Zhang, W.-B.; Wang, J.-Y.; Pei, J. Systematic Investigation of Side-Chain Branching Position Effect on Electron Carrier Mobility in Conjugated Polymers. *Adv. Funct. Mater.* **2014**, *24*, 6270−6278.
(24) Fu, B.; Baltazar, J.; Sankar, A. R.; Chu, P.-H.; Zhang, S.; Collard, D. M.; Reichmanis, E. Enhancing Field-Effect Mobility of Conjugated Polymers Through Rational Design of Branched Side Chains. *Adv. Funct. Mater.* **2014**, *24*, 3734−3744.
(25) Li, J.; Qiao, X.; Xiong, Y.; Li, H.; Zhu, D. Five-Ring Fused Tetracyanothienoquinoids as High-Performance and Solution-Processable n-Channel Organic Semiconductors: Effect of the Branching Position of Alkyl Chains. *Chem. Mater.* **2014**, *26*, 5782−5788.
(26) Meager, I.; Ashraf, R. S.; Mollinger, S.; Schroeder, B. C.; Bronstein, H.; Beatrup, D.; Vezie, M. S.; Kirchartz, T.; Salleo, A.; Nelson, J.; McCulloch, I. Photocurrent Enhancement from Diketopyrrolopyrrole Polymer Solar Cells through Alkyl-Chain Branching Point Manipulation. *J. Am. Chem. Soc.* **2013**, *135*, 11537−11540.
(27) Lei, T.; Wang, J.-Y.; Pei, J. Roles of Flexible Chains in Organic Semiconducting Materials. *Chem. Mater.* **2014**, *26*, 594−603.
(28) Mei, J.; Bao, Z. Side Chain Engineering in Solution-Processable Conjugated Polymers. *Chem. Mater.* **2014**, *26*, 604−615.
(29) Zhang, F.; Hu, Y.; Schuettfort, T.; Di, C.-A.; Gao, X.; McNeill, C. R.; Thomsen, L.; Mannsfeld, S. C. B.; Yuan, W.; Sirringhaus, H.; Zhu, D. Critical Role of Alkyl Chain Branching of Organic Semiconductors in Enabling Solution-Processed n-Channel Organic Thin-Film Transistors with Mobility of up to 3.50 $cm^2 V^{-1} s^{-1}$. *J. Am. Chem. Soc.* **2013**, *135*, 2338−2349.
(30) Sonar, P.; Singh, S. P.; Li, Y.; Soh, M. S.; Dodabalapur, A. A Low-Bandgap Diketopyrrolopyrrole-Benzothiadiazole-Based Copolymer for High-Mobility Ambipolar Organic Thin-Film Transistors. *Adv. Mater.* **2010**, *22*, 5409−5413.
(31) Bronstein, H.; Chen, Z.; Ashraf, R. S.; Zhang, W.; Du, J.; Durrant, J. R.; Shakya Tuladhar, P.; Song, K.; Watkins, S. E.; Geerts, Y.; Wienk, M. M.; Janssen, R. A. J.; Anthopoulos, T.; Sirringhaus, H.; Heeney, M.; McCulloch, I. Thieno[3,2-*b*]thiophene-Diketopyrrolopyrrole-Containing Polymers for High-Performance Organic Field-Effect Transistors and Organic Photovoltaic Devices. *J. Am. Chem. Soc.* **2011**, *133*, 3272−3275.
(32) Chen, Z.; Lee, M. J.; Shahid Ashraf, R.; Gu, Y.; Albert-Seifried, S.; Meedom Nielsen, M.; Schroeder, B.; Anthopoulos, T. D.; Heeney, M.; McCulloch, I.; Sirringhaus, H. High-Performance Ambipolar Diketopyrrolopyrrole-Thieno[3,2-*b*]thiophene Copolymer Field-Effect Transistors with Balanced Hole and Electron Mobilities. *Adv. Mater.* **2012**, *24*, 647−652.
(33) Lee, J.; Han, A.-R.; Yu, H.; Shin, T. J.; Yang, C.; Oh, J. H. Boosting the Ambipolar Performance of Solution-Processable Polymer Semiconductors via Hybrid Side-Chain Engineering. *J. Am. Chem. Soc.* **2013**, *135*, 9540−9547.
(34) Hao, Z.; Iqbal, A. Some Aspects of Organic Pigments. *Chem. Soc. Rev.* **1997**, *26*, 203−213.
(35) Lin, H.-W.; Lee, W.-Y.; Chen, W.-C. Selenophene-DPP Donor-Acceptor Conjugated Polymer for High Performance Ambipolar Field Effect Transistor and Nonvolatile Memory Application. *J. Mater. Chem.* **2012**, *22*, 2120−2128.
(36) Naik, M. A.; Patil, S. Diketopyrrolopyrrole-Based Conjugated Polymers and Small Molecules for Organic Ambipolar Transistors and Solar Cells. *J. Polym. Sci., Part A: Polym. Chem.* **2013**, *51*, 4241−4260.
(37) García, G.; Granadino-Roldán, J. M.; Hernández-Laguna, A.; Garzón, A.; Fernández-Gómez, M. A Tuned LRC-DFT Design of Ambipolar Diketopyrrolopyrrole-Containing Quinoidal Molecules Interesting for Molecular Electronics. *J. Chem. Theory Comput.* **2013**, *9*, 2591−2601.
(38) Han, A.-R.; Dutta, G. K.; Lee, J.; Lee, H. R.; Lee, S. M.; Ahn, H.; Shin, T. J.; Oh, J. H.; Yang, C. ε-Branched Flexible Side Chain Substituted Diketopyrrolopyrrole-Containing Polymers Designed for High Hole and Electron Mobilities. *Adv. Funct. Mater.* **2015**, *25*, 247−254.
(39) Kanimozhi, C.; Yaacobi-Gross, N.; Chou, K. W.; Amassian, A.; Anthopoulos, T. D.; Patil, S. Diketopyrrolopyrrole-Diketopyrrolopyrrole-Based Conjugated Copolymer for High-Mobility Organic Field-Effect Transistors. *J. Am. Chem. Soc.* **2012**, *134*, 16532−16535.
(40) Sun, B.; Hong, W.; Aziz, H.; Li, Y. A Pyridine-Flanked Diketopyrrolopyrrole (DPP)-Based Donor-Acceptor Polymer Showing High Mobility in Ambipolar and n-Channel Organic Thin Film Transistors. *Polym. Chem.* **2015**, *6*, 938−945.
(41) Kanimozhi, C.; Yaacobi-Gross, N.; Burnett, E. K.; Briseno, A. L.; Anthopoulos, T. D.; Salzner, U.; Patil, S. Use of Side-Chain for Rational Design of n-Type Diketopyrrolopyrrole-Based Conjugated Polymers: What did We Find out? *Phys. Chem. Chem. Phys.* **2014**, *16*, 17253−17265.
(42) Park, J. H.; Jung, E. H.; Jung, J. W.; Jo, W. H. A Fluorinated Phenylene Unit as a Building Block for High-Performance n-Type Semiconducting Polymer. *Adv. Mater.* **2013**, *25*, 2583−2588.
(43) Li, Y.; Sonar, P.; Murphy, L.; Hong, W. High Mobility Diketopyrrolopyrrole (DPP)-Based Organic Semiconductor Materials for Organic Thin Film Transistors and Photovoltaics. *Energy Environ. Sci.* **2013**, *6*, 1684−1710.
(44) Qiao, Y.; Guo, Y.; Yu, C.; Zhang, F.; Xu, W.; Liu, Y.; Zhu, D. Diketopyrrolopyrrole-Containing Quinoidal Small Molecules for High-Performance, Air-Stable, and Solution-Processable n-Channel Organic Field-Effect Transistors. *J. Am. Chem. Soc.* **2012**, *134*, 4084−4087.
(45) Wang, C.; Zang, Y.; Qin, Y.; Zhang, Q.; Sun, Y.; Di, C.-A.; Xu, W.; Zhu, D. Thieno[3,2-b]thiophene-Diketopyrrolopyrrole-Based Quinoidal Small Molecules: Synthesis, Characterization, Redox Behavior, and n-Channel Organic Field-Effect Transistors. *Chem. - Eur. J.* **2014**, *20*, 13755−13761.
(46) Uno, M.; Seto, K.; Takahashi, S. A New Method of Synthesis of Arylmalononitriles catalyzed by a Palladium Complex. *J. Chem. Soc., Chem. Commun.* **1984**, 932−933.
(47) Yui, K.; Ishida, H.; Aso, Y.; Otsubo, T.; Ogura, F.; Kawamoto, A.; Tanaka, J. Novel Electron Acceptors Bearing a Heteroquinonoid System. II. Synthesis and Conductive Complexes of 2,5-Bis-(dicyanomethylene)-2,5-dihydrothieno-[3,2-b]thiophene, 2,6-Bis-(dicyanomethylene)-2,6-dihydrodithieno[3,2-b:2′,3′-d]thiophene, and Their Derivatives. *Bull. Chem. Soc. Jpn.* **1989**, *62*, 1547−1555.
(48) Babel, A.; Jenekhe, S. A. Alkyl Chain Length Dependence of the Field-Effect Carrier Mobility in Regioregular Poly(3-alkylthiophene)s. *Synth. Met.* **2005**, *148*, 169−173.
(49) Park, Y. D.; Kim, D. H.; Jang, Y.; Cho, J. H.; Hwang, M.; Lee, H. S.; Lim, J. A.; Cho, K. Effect of Side Chain Length on Molecular

DOI: 10.1021/acsami.5b04082
ACS Appl. Mater. Interfaces 2015, 7, 15978−15987

Ordering and Field-Effect Mobility in Poly(3-alkylthiophene) Transistors. *Org. Electron.* **2006**, *7*, 514−520.

DOI: 10.1021/acsami.5b04082
ACS Appl. Mater. Interfaces 2015, 7, 15978−15987